Inorg. Chem. **2007**, *46*, 2998–3009

pH-Specific Synthesis and Spectroscopic, Structural, and Magnetic Studies of a Chromium(III)–Citrate Species. Aqueous Solution Speciation of the Binary Chromium(III)–Citrate System

C. Gabriel,[†] C. P. Raptopoulou,[‡] A. Terzis,[‡] V. Tangoulis,[§] C. Mateescu,[||] and A. Salifoglou*[,†]

Department of Chemical Engineering, Laboratory of Inorganic Chemistry, Aristotle University of Thessaloniki, Thessaloniki 54124, Greece, Chemical Process Engineering Research Institute, Thermi, Thessaloniki 57001, Greece, Institute of Materials Science, NCSR "Demokritos", Aghia Paraskevi 15310, Attiki, Greece, Department of Materials Science, University of Patras, Patras 26500, Greece, and Banat University of Agricultural Sciences and Veterinary Medicine, Timisoara 1900, Romania

Received August 7, 2006

In an attempt to understand the aqueous interactions of Cr(III) with the low-molecular-mass physiological ligand citric acid, the pH-specific synthesis in the binary Cr(III)–citrate system was explored, leading to the complex $(NH_4)_4[Cr(C_6H_4O_7)(C_6H_5O_7)]\cdot 3H_2O$ (**1**). **1** crystallizes in the monoclinic space group *I*2/*a*, with $a = 19.260(10)$ Å, $b = 10.006(6)$ Å, $c = 23.400(10)$ Å, $\beta = 100.73(2)°$, $V = 4431(4)$ Å^3, and $Z = 8$. **1** was characterized by elemental analysis and spectroscopic, structural, thermal, and magnetic susceptibility studies. Detailed aqueous speciation studies in the Cr(III)–citrate system suggest the presence of a number of species, among which is the mononuclear $[Cr(C_6H_4O_7)(C_6H_5O_7)]^{4-}$ complex, optimally present around pH $\approx$ 5.5. The structure of **1** reveals a mononuclear octahedral complex of Cr(III) with two citrate ligands bound to it. The two citrate ligands have different deprotonation states, thus signifying the importance of the mixed deprotonation state in the coordination sphere of the Cr(III) species in aqueous speciation. The latter reveals the distribution of numerous species, including **1**, for which the collective structural, spectroscopic, and magnetic data point out its physicochemical profile in the solid state and in solution. The importance of the synthetic efforts linked to **1** and the potential ramifications of Cr(III) reactivity toward both low- and high-molecular-mass biotargets are discussed in light of (a) the quest for well-characterized soluble Cr(III) species that could be detected and identified in biologically relevant fluids, (b) ongoing efforts to delineate the aqueous speciation of the Cr(III)–citrate system and its link to biotoxic Cr(III) manifestations, and (c) the synthetic utility of convenient Cr(III) precursors in the synthesis of advanced materials.

Introduction

Chromium is an abundant element in the earth's crust. It is present in both abiotic and biological systems.[1] As a metal, it is used in various industrial processes in tanneries and the cement, plating, and alloying industries, as well as in corrosive paints.[2] It is also used as a dopant[3] to improve the nonlinear optical properties of key oxide materials,[4] modifying the efficiency and lifetime of the photorefractive signals (i.e., the "memory"-type signals in connection with hologram recording).[5] Equally significant is the presence of chromium in binary metal oxides, finding applications in heterogeneous catalysts; electrochromic devices; and, more recently, gas sensors.[6]

In the biological world, chromium is encountered in plants and animals. Chromium involvement has been reported in

* Author to whom correspondence should be addressed. Tel.: +30-2310-996-179. Fax: +30-2310-996-196. E-mail: salif@auth.gr.

[†] Aristotle University of Thessaloniki and Chemical Process Engineering Research Institute.

[‡] NCSR "Demokritos".

[§] University of Patras.

[||] Banat University of Agricultural Sciences and Veterinary Medicine.

(1) Bae, W.-C.; Lee, H.-K.; Choe, Y.-C.; Jahng, D.-J.; Lee, S.-H.; Kim, S.-J.; Lee, J.-H.; Jeong, B.-C. *J. Microbiol.* **2005**, *43*, 21−27.

(2) Ramos, R. L.; Martinez, A. J.; Coronado, R. M. G. *Water Sci. Technol.* **1994**, *30*, 191.

(3) Pèter, À.; Szakács, O.; Fö1dvári, I.; Bencs, L.; Munoz, A. F. *Mater. Res. Bull.* **1996**, *31*, 1067.

(4) Fö1dvári, I.; Scripsick, M. P.; Halliburton, L. E.; Pèter, À. *Phys. Lett. A* **1991**, *154*, 84.

(5) Fö1dvári, I.; Pèter, À.; Powell, R. C.; Taheri, B. *Opt. Mater.* **1995**, *4*, 299.

10.1021/ic061480j CCC: $37.00
Published on Web 03/23/2007

nucleic acid synthesis.[7] In mammals, chromium is associated with the low-molecular-weight chromium-binding substance chromodulin,[8,9] playing a pivotal role in glucose homeostasis and lipid metabolism through potentiation of insulin action. To this end, low-molecular-mass chromium complexes, such as chromium picolinate, are often used as dietary supplements[10a] to sustain normal physiology, improve insulin sensitivity, and correct dyslipidemia. Toxicity associated with such chromium compounds, however, has been a subject of major concern[10b] and has compromised their therapeutic value.

In the environment, Cr(VI) is highly water soluble, inducing major carcinogenic and mutagenic processes upon cellular internalization.[11,12] Cr(III) solution chemistry,[13] on the other hand, in diverse cellular media containing a plethora of solubilizing substrates (peptides, proteins, α-hydroxycarboxylates, etc.), indicates that it is responsible for the generation of Cr(III)−DNA cross links linked to Cr(VI)-induced carcinogenicity in Cr(VI)-exposed cells.[11,12] In vitro tests have shown that soluble Cr(III) is a potential toxin, because it can act as a competitive inhibitor of many cellular processes.[14] The potential roles of Cr(III) in biological systems are most likely linked to its binary and ternary interactions with lipids, proteins, and amino acids free in the cytosol or as components of peptides and lipid membrane structures. Poised to understand the Cr(III)−(α-hydroxycarboxylate) interactions in cellular processes, we have launched efforts targeting (a) the aqueous synthesis of Cr(III) complexes in the presence of metal-complexing carboxylate-containing low-molecular-mass physiological ligands and (b) the solution structural speciation of the Cr(III) binary system of species potentially becoming bioavailable toward cellular targets. In this respect, we report herein solution speciation studies of the binary Cr(III)−citrate system and the pH-specific synthesis and physicochemical characterization of an aqueous Cr(III)−citrate species emerging from the associated speciation.

Experimental Section

Materials and Methods. All experiments were carried out in the open air. Nanopure-quality water was used for all reactions. $Cr(NO_3)_3 \cdot 9H_2O$ and citric acid monohydrate were purchased from Aldrich. Ammonia was supplied by Fluka.

Physical Measurements. FT-IR spectra were recorded on a Perkin-Elmer 1760X FT-IR spectrometer. UV−visible measurements were carried out on a Hitachi U2001 spectrophotometer in the range from 190 to 1000 nm. A ThermoFinnigan Flash EA 1112 CHNS elemental analyzer was used for the simultaneous determination of carbon, hydrogen, and nitrogen (%). The analyzer is based on the dynamic flash combustion of the sample (at 1800 °C), followed by reduction, trapping, complete GC separation, and detection of the products. The instrument is fully automated and controlled by PC via the Eager 300 dedicated software. The instrument is capable of handling solid, liquid, or gaseous substances.

A TA Instruments thermal analyzer system, model Q 600, was used to run the simultaneous TGA−DSC experiments. The instrument mass precision is 0.1 μg, and the heating rate employed was 5 °C/min. About 18.5 mg of sample was placed in an open alumina sample pan for each experiment. High-purity helium and air (80/20 in N_2/O_2) were used at a constant flow rate of 100 mL/min, depending on the conditions required for running the experiment(s). During the experiments, the sample weight loss and rate of weight loss were recorded continuously under dynamic conditions, as a function of time or temperature, in the range 30−1000 °C. Before the heating routine program was activated, the entire system was purged with the appropriate gas for 10 min at a rate 400 mL/min, to ensure that the desired environment was established.

The EPR spectra of complex **(1)** in the solid state and in aqueous solutions were recorded on a Bruker ER 200D-SRC X-band spectrometer, equipped with an Oxford ESR 9 cryostat at 9.43 GHz and 10 dB and in the range 4−150 K. Magnetic susceptibility data were collected on powdered samples of **1** with a Quantum Design SQUID susceptometer in the 2−300 K temperature range, under various applied magnetic fields. Magnetization measurements were carried out at two different temperatures in the field range of 0−5 T.

pH-Potentiometric Measurements. The protonation constants of citric acid were determined by pH-potentiometric titrations of 30-mL samples in the pH range 2.5−11 under a purified argon atmosphere. The concentration of citric acid was in the range of 1.7−7.0 mmol dm^{-3}. The stability constants of the Cr(III) complexes of citric acid were determined by pH-potentiometric titrations of 30-mL samples in the pH range 2.5−11.2 under a purified argon atmosphere. All solutions were prepared using Fluka reagent-grade citric acid, $Cr(NO_3)_3 \cdot 9H_2O$, and ultrapure deionized water. The purity of the citric acid and the exact concentrations of the citrate and chromium solutions were determined by the Gran method.[15] To avoid chromium hydrolysis, aqueous solutions of chromium nitrate were prepared in 0.01 M nitric acid. The exact concentration of chromium was checked by the method of Kinnunen et al.[16]

The ionic strength was adjusted to 0.15 M with NaCl. The temperature was maintained at 25.0 ± 0.1 °C during the measurements. The titrations were carried out with a carbonate-free NaOH solution of known concentration (ca. 0.15 M). The NaOH solution was standardized using potassium hydrogen iodate [$KH(IO_3)_2$]. The ligand concentration was 1.7 mM, and the metal/ligand ratios employed were 1:1, 1:2, 1:3, and 1:4. The pH was measured with a computer-controlled Crison titration system elaborated for titra-

(6) (a) Moseley, T.; Norris, J. O. W.; Williams, E. *Techniques and Mechanisms in Gas Sensing*; Adam Hilger Series on Sensors; I.O.P. Publishing: Bristol, U.K., 1991. (b) Schierbaum, K. D.; Weimar, U.; Gopel, W. *Sens. Actuators B* **1991**, *3*, 205−214. (c) Meixner, H.; Lampe U. *Sens. Actuators B* **1996**, *33*, 198−202.
(7) Richard, F. C.; Bourg, A. C. M. *Water Res.* **1991**, *25*, 807.
(8) (a) Vincent, J. B. *Acc. Chem. Res.* **2000**, *33*, 503−510. (b) Davis, C. M.; Vincent, J. B. *Arch. Biochem. Biophys.* **1997**, *339*, 335−343.
(9) (a) Vincent, J. B. *Polyhedron* **2001**, *20*, 1−26. (b) Davis, C. M.; Vincent, J. B. *Biochemistry* **1997**, 36, 4382−4385.
(10) (a) Stephen Morris, G.; Guidry, K. A.; Hegsted, M.; Hasten, D. L. *Nutr. Res.* **1995**, *15*, 1045−1052. (b) Stearns, D. M.; Wise, J. P., Sr.; Patierno, S. R.; Wetterhahn, K. E. *FASEB J.* **1995**, *9*, 1643−1648.
(11) (a) Levina, A.; Lay, P. A. *Coord. Chem. Rev.* **2005**, *249*, 281−288. (b) Pettrilli, F. L.; Miller, W. *Appl. Environ. Microbiol.* **1977**, *33*, 805−809.
(12) (a) Levina, A.; Codd, R.; Dillon, C. T.; Lay, P. A. *Prog. Inorg. Chem.* **2003**, *51*, 145−250. (b) Levis, A. G.; Bianchi, V. In *Biological and Environmental Aspects of Chromium*; Langard, S., Ed.; Elsevier Science: Amsterdam, 1982; pp 171−208.
(13) Wang, Y. T.; Shen, H. *J. Ind. Microbiol.* **1995**, *14*, 159−164.
(14) Walsh, A. R.; O'Halloran, J.; Gower, A. M. *Ecotoxicol. Environ. Saf.* **1994**, *27*, 168.
(15) (a) Gran, G. *Acta Chem. Scand.* **1950**, *29*, 559. (b) Gran, G. *Analyst* **1952**, *77*, 661−671. (c) Rossotti, F. J. C.; Rossotti, H. *J. Chem. Educ.* **1965**, *42*, 375−378.
(16) Kinnunen, J.; Wennerstrand, B. *Chem.-Anal.* **1955**, *44*, 33.

tions at such low concentrations[17] and a Mettler Toledo-Inlab 412 combined glass electrode, calibrated for hydrogen ion concentration according to Irving et al.,[18] by using the GLEE program.[19] The ion product of water was found to be $pK_w = 13.76$.

The stepwise protonation constants of citric acid are given as $\log K_n$ ($n = 1-3$), consistent with the equilibrium $H_{n-1}L + H \rightleftarrows H_nL$, where $K_n = [H_nL]/[H_{n-1}L][H]$. The initial computations were obtained in the form of overall protonation constants $\beta_n = [H_nL]/[L][H]^n$, taking into account the relation $\beta_n = \prod_{n=1}^{n=3} K_n$.

The concentration stability constants $\beta_{pqr} = [M_pL_qH_r]/[M]^p[L]^q[H]^r$ for citric acid were calculated with Superquad,[20] and those for the Cr(III)−citrate complexes formed in the investigated system were calculated with the PSEQUAD computer program.[21] Species distribution diagrams were computed from the overall formation constants with HySS.[22]

The formation of hydroxo complexes of Cr(III) was taken into account in the calculations. Overall Cr(III) hydrolysis constant values are defined as $\beta_{xy} = [Cr_x(OH)_y][H]^y/[Cr]^x$.[23a] To this end, the following species were considered: $[Cr(OH)]^{2+}$ ($\log \beta_{1-1} = -4.42$), $[Cr_2(OH)_2]^{4+}$ ($\log \beta_{2-2} = -4.81$), and $[Cr_3(OH)_4]^{5+}$ ($\log \beta_{3-4} = -8.08$), with stability constants calculated from the data of Baes et al.[23b] and corrected for an ionic strength of 0.15 M by use of the Davis equation, and $[Cr(OH)_2]^+$ ($\log \beta_{1-2} = -9.7$), $[Cr(OH)_3]^0$ ($\log \beta_{1-3} = -18.0$), and $[Cr(OH)_4]^-$ ($\log \beta_{1-4} = -27.8$) taken from Baes et al.[23b]

Preparation of Complex $(NH_4)_4[Cr(C_6H_4O_7)(C_6H_5O_7)]\cdot 3H_2O$ (1). A quantity of $Cr(NO_3)_3\cdot 9H_2O$ (0.80 g, 1.0 mmol) was placed in a flask and dissolved in 2.5 mL of H_2O. Subsequently, citric acid (0.84 g, 2.0 mmol) was added slowly under continuous stirring. Aqueous ammonia was then added slowly to adjust the pH to a final value of ∼5.5. The resulting solution was left stirring overnight. Addition of cold ethanol at 4 °C resulted, after a couple of months, in the deposition of a blue-colored crystalline material. The crystals were isolated by filtration and dried in vacuo. The yield of the reaction was 0.33 g (30%). Anal. Calcd for **1**, $(NH_4)_4[Cr(C_6H_4O_7)(C_6H_5O_7)]\cdot 3H_2O$ ($C_{12}H_{31}O_{17}N_4Cr$, MW 555.41): C, 25.95; H, 5.59; N, 10.09. Found: C, 25.68; H, 5.45; N, 9.93.

X-ray Crystal Structure Determination. X-ray-quality crystals of compound **1** were grown from mixtures of water−ethanol solutions. A single crystal of **1**, with dimensions 0.05 × 0.10 × 0.20 mm, was mounted on a $P2_1$ Nicolet diffractometer upgraded by Crystal Logic, using graphite-monochromated CuK_α radiation. Unit cell dimensions for **1** were determined and refined using the angular settings of 25 automatically centered reflections in the range $22° < 2\theta < 54°$. Crystallographic details are reported in Table 1. Intensity data were measured using $\theta-2\theta$ scans. Throughout data collection, three standard reflections were monitored for every 97 reflections and showed less than 3% variation and no decay. Lorentz, polarization, and ψ-scan absorption corrections were applied using Crystal Logic software. Further experimental crystallographic details for **1**: $2\theta_{max} = 118°$, scan speed = 3°/min, scan range = 2.35 + $\alpha_1\alpha_2$ separation, number of reflections collected/unique/used = 3250/3158[R(int) = 0.0741]/3158, 412 parameters refined, $F(000) = 2328$, $(\Delta/\sigma)_{max} = 0.002$, $(\Delta\rho)_{max}/(\Delta\rho)_{min} = 0.528/-0.475$ e/Å^3, GOF = 1.061, R/R_w (for all data) = 0.0480/0.1083.

Table 1. Summary of Crystal, Intensity Collection, and Refinement Data for $(NH_4)_4[Cr(C_6H_4O_7)(C_6H_5O_7)]\cdot 3H_2O$ **(1)**

	1
formula	$C_{12}H_{31}N_4O_{17}Cr$
formula weight	555.41
T (K)	293(2)
wavelength (Å)	Cu Kα, 1.54180
space group	$I2/a$
a (Å)	19.260(10)
b (Å)	10.006(6)
c (Å)	23.400(10)
α (deg)	90.00
β (deg)	100.73(2)
γ (deg)	90.00
V (Å^3)	4431(4)
Z	8
D_{calcd}/D_{measd} (Mg m^{-3})	1.665/1.67
abs coeff, μ (mm^{-1})	5.102
ranges of h, k, l	$-20 \le h \le 21$, $0 \le l \le 11$, $-26 \le k \le 0$
GOF on F^2	1.061
R indices[a]	$R = 0.0412$, $R_w = 0.1022$[b]

[a] R values are based on F; R_w values are based on F^2. $R = \sum||F_o| - |F_c||/\sum(|F_o|)$; $R_w = \{\sum[w(F_o^2 - F_c^2)^2]/\sum[w(F_o^2)^2]\}^{1/2}$. [b] 2784 reflections with $I > 2\sigma(I)$.

Results

Synthesis. The synthesis of compound **1** was expediently pursued through a facile reaction between Cr(III) and citric acid in aqueous solutions. The pH at which the reaction occurred was 5.5. Ammonia was used as a base for the adjustment of the pH of the reaction mixture and the concurrent generation of the counterion for the assembled anionic complex. This phenomenon has been observed on a number of occasions in metal−citrate chemistry. The stoichiometric reaction leading to the formation of the title compound is given by reaction 1.The compound was isolated

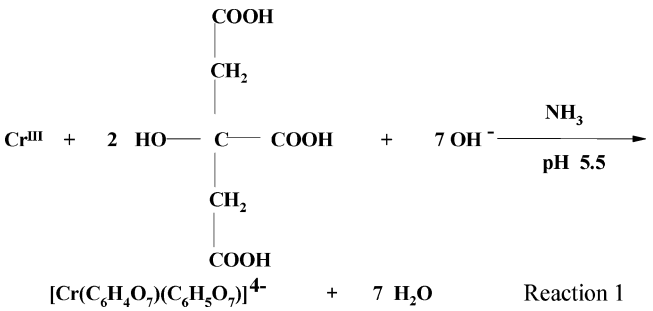

(17) Micro TT2050 Titrator Quick Guide, Crison Instruments, Alella, Spain, 1985.
(18) Irving, H. M.; Miles, M. G.; Petit, L. D. *Anal. Chim. Acta* **1967**, *38*, 475−479.
(19) Gans, P.; O'Sullivan, B. *Talanta* **2000**, *51*, 33−37.
(20) Gans, P.; Sabatini, A.; Vacca, A. *J. Chem. Soc., Dalton Trans.* **1985**, 1195.
(21) Zékány, L.; Nagypál, I.; Peintler, G. *PSEQUAD for Chemical Equilibria*; Technical Software Distributions: Baltimore, MD, 1991.
(22) Alderighi, L.; Gans, P.; Ienco, A.; Peters, D.; Sabatini, A.; Vacca, A. *Coord. Chem. Rev.* **1999**, *184*, 311−318.
(23) (a) Lacour, S.; Deluchat, V.; Bollinger, J.-C.; Serpaud, B. *Talanta* **1998**, *46*, 999−1009. (b) Baes, C. F., Jr.; Mesmer, R. E. In *The Hydrolysis of Cations*; Wiley-Interscience Publishers: New York, 1976.
(24) Sheldrick, G. M. *SHELXS-86: Program for the Solution of Crystal Structures*; University of Göttingen: Göttingen, Germany, 1986.
(25) Sheldrick, G. M. *SHELXL-97: Program for the Refinement of Crystal Structures*; University of Göttingen: Göttingen, Germany, 1997.

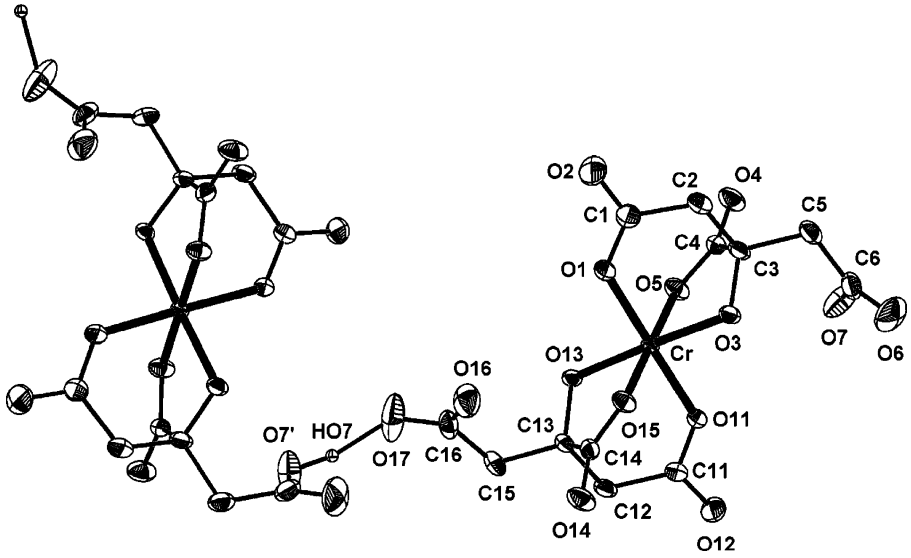

Figure 1. ORTEP structure of the $[Cr(C_6H_4O_7)(C_6H_5O_7)]^{4-}$ anion with the atom labeling scheme in **1**. Thermal ellipsoids are drawn by ORTEP and represent 50% probability surfaces. The formation of hydrogen-bonded chains along the *a* axis is also shown.

Table 2. Bond Lengths (Å) and Angles (deg) in $(NH_4)_4[Cr(C_6H_4O_7)(C_6H_5O_7)]\cdot 3H_2O$ (**1**)

	Distances		
Cr−O(3)	1.933(2)	Cr−O(15)	1.977(2)
Cr−O(13)	1.946(2)	Cr−O(1)	1.990(2)
Cr−O(5)	1.974(2)	Cr−O(11)	1.993(2)
	Angles		
O(3)−Cr−O(13)	177.73(8)	O(5)−Cr−O(1)	89.31(9)
O(3)−Cr−O(5)	82.55(9)	O(15)−Cr−O(1)	91.35(9)
O(13)−Cr−O(5)	97.27(9)	O(3)−Cr−O(11)	89.88(9)
O(3)−Cr−O(15)	97.51(9)	O(13)−Cr−O(11)	87.86(9)
O(13)−Cr−O(15)	82.65(9)	O(5)−Cr−O(11)	90.13(9)
O(5)−Cr−O(15)	179.34(9)	O(15)−Cr−O(11)	89.21(9)
O(3)−Cr−O(1)	89.26(9)	O(1)−Cr−O(11)	179.02(8)
O(13)−Cr−O(1)	93.01(9)		

in pure crystalline form upon addition of ethanol to the reaction mixture at 4 °C. Elemental analysis of the isolated bluish crystalline material suggested the molecular formulation $(NH_4)_4[Cr(C_6H_4O_7)(C_6H_5O_7)]\cdot 3H_2O$ for **1**. Further spectroscopic inspection of **1** by FT−IR spectrocopy revealed the presence of citrate bound to Cr(III), thus affirming the proposed formulation.

Compound **1** is soluble in water. It is insoluble in organic solvents, such as methanol, acetonitrile, chlorinated solvents ($CHCl_3$, CH_2Cl_2), toluene, and DMF. The material is stable in the air at room temperature for a long period of time.

Description of the Structure of $(NH_4)_4[Cr(C_6H_4O_7)(C_6H_5O_7)]\cdot 3H_2O$ (1). The X-ray crystal structure of **1** reveals the presence of discrete cations and anions in the lattice. The compound crystallizes in the monoclinic space group *I*2/*a*. The ORTEP diagram of **1** is shown in Figure 1. Selected interatomic distances and bond angles for **1** are listed in Table 2. The structure consists of a mononuclear core unit composed of a central Cr(III) ion surrounded by two citrate ligands. The citrate ligands bind to the metal ion through the central carboxylate and alkoxide oxygens, promoting the formation of a stable metallacyclic ring. An additional carboxylate oxygen from one of the terminal carboxylates of each citrate ligand binds the central metal ion, thus occupying a third coordination site around Cr(III). The second terminal carboxylate group of each citrate does not bind Cr(III). Therefore, the six coordination sites around Cr(III) are taken up by the two citrate ligands bound in the same fashion. The geometry arising from the described citrate coordination is distorted octahedral.

Worth mentioning in regard to the structure of this Cr(III) species is the state of deprotonation of the two bound citrate ligands. A similar behavior with metal-bound citrate ligands of varying protonation states was previously observed in the cases of Al(III) and Ga(III). Specifically, the complexes $(NH_4)_4[Al(C_6H_4O_7)(C_6H_5O_7)]\cdot 3H_2O$[26] and $(NH_4)_4[Ga(C_6H_4O_7)(C_6H_5O_7)]\cdot 3H_2O$[26] contain similar coordination environments generated by two citrate ligands differing in their (de)protonation states. In comparison to complex **1**, containing two Cr(III)-bound citrate ligands with variable states of deprotonation, the only other known chromium(III)−citrate species, $(C_5H_6N)_2[Cr(C_6H_{5.5}O_7)_2]\cdot 4H_2O$ (**2**),[27] exhibits two Cr(III)-bound citrate ligands with the same degree of (de)protonation. In fact, each citrate ion in **2** contains a protonated terminal carboxylate group, whereas the alkoxide oxygen appears to have a hydrogen atom shared equally between the two citrate ligands. Thus, the formal charge of each citrate ligand in complex **2** is 2.5 (vide infra). As a result, the charge on the anionic complex **2** is 2−, as opposed to 4− in the corresponding complex **1**. The latter bears one triply and one quadruply deprotonated citrate ligand, with the alcoholic moieties being deprotonated. Beyond these differences in the anionic assembly, the counterion in **1** is ammonium, whereas the counterion in complex **2** is a pyridinium ion.

The Cr−O bond distances in **1** are in line with those in other Cr(III) oxygen-containing complexes, such as $(C_5H_6N)_2[Cr(C_6H_{5.5}O_7)_2]\cdot 4H_2O$ (**2**) [1.965(2)−1.987(2) Å],[27] $Na_2[Cr-$

(26) Matzapetakis, M.; Kourgiantakis, M.; Danakali, M.; Raptopoulou, C. P.; Terzis, A.; Lakatos, A.; Kiss, T.; Banyai, I.; Iordanidis, L.; Mavromoustakos, T.; Salifoglou, A. *Inorg. Chem.* **2001**, *40*, 1734−1744.

(27) Quiros, M.; Goodgame, D. M. L.; Williams, D. J. *Polyhedron* **1992**, *11*, 1343−1348.

$(C_5H_7NO_4)_2]$ (**3**) [1.963(2)−1.948(2) Å],[28] $K_3[Cr(C_2O_4)_3]\cdot 3H_2O$ (**4**) [1.955(2)−1.985(2) Å],[29] $K_2[Cr_2(C_6H_6NO_6)_2(OH)_2]\cdot 6H_2O$ (**5**) [1.937(4)−1.983(3) Å],[30] *trans*-(O_5)−Na[Cr(ed3ap)]·$3H_2O$ (**6**) (ed3ap = ethylenediamine-*N*,*N*,*N*′-triacetate-*N*′-3-propionate) [1.945(6)−1.974(5) Å],[31] and $[Cr(ed3a)(H_2O)]\cdot H_2O$ (**7**) (ed3a = ethylenediamine-*N*,*N*,*N*′-triacetate) [1.947(2)−1.979(2) Å],[32] and trivalent metal−citrate complexes such as $(NH_4)_4[Al(C_6H_4O_7)(C_6H_5O_7)]\cdot 3H_2O$ (**8**) [1.836(1)−1.959(1) Å] and $(NH_4)_4[Ga(C_6H_4O_7)(C_6H_5O_7)]\cdot 3H_2O$ (**9**) [1.893(1)−2.058(1) Å]. It appears that angles similar to those in **1** are observed in a number of Cr(III)-O_6-core-containing complexes exhibiting an octahedral geometry around the Cr(III) ions. Among such complexes are **2** [81.5(1)−88.7(1)°], **4** [81.8(1)−98.9(1)°], and $[Cr(C_9H_{12}N_2O_6COOH)(H_2O)]$ (**10**) [89.43(8)−97.10(10)°].[33]

Considering the citrate moiety bound to the metal ion in compound **1**, the carbon atoms C(1), C(2), C(3), C(5), and C(6) of the citrate backbone are coplanar, with the largest standard deviation being 0.11 Å for C(3). The O(3)−C(3)−C(4) plane of the central carboxylate group is rotated by 19.1° out of the O(4)−C(4)−O(5) plane. The terminal carboxylate planes O(1)−C(1)−O(2) and O(6)−C(6)−O(7) are rotated by 10.9° and 60.2°, respectively, from the C(1)−C(2)−C(3)−C(5)−C(6) plane. The angle between the terminal carboxylate planes O(1)−C(1)−O(2) and O(6)−C(6)−O(7) is 63.9°. In the second citrate ligand, the carbon atoms of the citrate backbone are coplanar as well, with the largest deviation being 0.03 Å for C(12). The O(13)−C(13)−C(14) plane of the central carboxylate group is rotated by 12.8° out of the O(14)−C(14)−O(15) plane. The terminal carboxylate planes O(11)−C(11)−O(12) and O(16)−C(16)−O(17) are rotated by 9.9° and 33.1°, respectively, from the C(11)−C(12)−C(13)−C(15)−C(16) plane. The angle between the terminal carboxylate planes O(11)−C(11)−O(12) and O(16)−C(16)−O(17) is 40.9°.

The presence of protonated terminal carboxylates in the structure of **1** plays a key role in the development of its lattice structure. The terminal protonated carboxylate group of one of the bound citrate ligands is strongly hydrogen-bonded to a deprotonated terminal carboxylate group of an adjacent complex anion [HO(17)···O(7′) = 1.580 Å, O(17)···O(7′) = 2.540 Å, HO(17)−O(17)···O(7′) = 166.6°; ′ = 0.5 + *x*, −*y*, *z*]. As a result, polymeric chains of the anion of **1** are formed along the *a* axis. The ammonium counterions, the lattice water molecules, and the carboxylate groups of the citrate ligands participate in the formation of an extensive network of hydrogen bonds (Supporting Information), which very likely contributes to the stability of the crystal lattice in **1**.

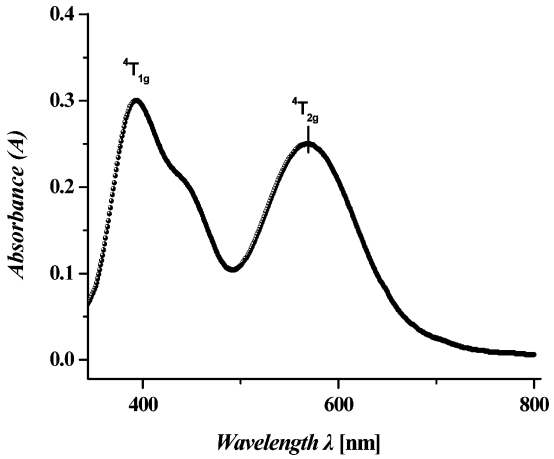

Figure 2. UV−visible spectrum of $(NH_4)_4[Cr(C_6H_4O_7)(C_6H_5O_7)]\cdot 3H_2O$ (**1**), in the range 350−800 nm, in water. The concentration of the sample is $c = 9$ mM.

Electronic Spectroscopy. The UV−visible spectrum of **1** was taken in water (Figure 2). The spectrum shows a band around $\lambda_{max} = 570$ nm ($\epsilon = 27.8$ M^{-1} cm^{-1}). At higher energies, a shoulder-like band appears at 450 nm ($\epsilon \approx 22$ M^{-1} cm^{-1}), ultimately reaching a well-formed major peak at $\lambda_{max} = 393$ nm ($\epsilon = 33.3$ M^{-1} cm^{-1}). A very weak shoulder-like band appears at 318 nm ($\epsilon \approx 9$ M^{-1} cm^{-1}) subsequently rising into the UV region. In the ultraviolet region, a clear band appears at 270 nm ($\epsilon = 244.5$ M^{-1} cm^{-1}). The absorption features are likely due to d−d transitions, which are typical for a Cr(III) d^3 (^4F) octahedral species.[34] The band around 570 nm could be tentatively attributed to the $^4A_{2g} \rightarrow {}^4T_{2g}$ transition. In an analogous fashion, the band at 393 nm could be assigned to the $^4A_{2g} \rightarrow {}^4T_{1g}(F)$ transition. The band at 270 nm could be tentatively assigned to the $^4A_{2g} \rightarrow {}^4T_{1g}(P)$ transition.[35] No further definitive assignments could be made in the absence of detailed specific studies. The spectrum of **1** in water is different from that of Cr(III)(aq),[36] indicating that the coordination sphere of Cr(III) in **1** is likely to be retained in solution.

FT−IR Spectroscopy. The FT-IR spectrum of **1** in KBr revealed the presence of vibrationally active carboxylate groups. Both antisymmetric and symmetric vibrations for the carboxylate groups of the coordinated citrate ligands were present. Specifically, antisymmetric stretching vibrations, $\nu_{as}(COO^-)$, for the carboxylate carbonyls appeared in the range 1653−1574 cm^{-1}. Symmetric vibrations, $\nu_s(COO^-)$, for the same groups appeared in the range 1436−1352 cm^{-1}. The frequencies of the observed carbonyl vibrations were shifted to lower values in comparison to the corresponding vibrations in free citric acid, indicating changes in the

(28) Suh, J.-S.; Park, S.-J.; Lee, K.-W.; Suh, I.-H.; Lee, J.-H.; Song, J.-H.; Oh, M.-R. *Acta Crystallogr.* **1997**, *C53*, 432−434.
(29) Taylor, D. *Aust. J. Chem.* **1978**, *31*, 1455−1462.
(30) Choi, J.-H.; Suzuki, T.; Kaizaki, S. *Acta Crystallogr.* **2003**, *E59*, m812−m813.
(31) Radanovic, D. J.; Sakagami, N.; Ristanovic, V. M.; Kaizaki, S. *Inorg. Chim. Acta* **1999**, *292*, 16−27.
(32) Grubisic, S.; Gruden-Pavlovic, M.; Niketic, S. R; Kaizaki, S.; Sakagami-Yoshida, N. *Inorg. Chem. Commun.* **2003**, *6*, 1180−1184.
(33) Gerdom, L. E.; Baenziger, N. A.; Goff, H. M. *Inorg. Chem.* **1981**, *20*, 1606−1609.
(34) Drago, R. S. *Physical Methods in Chemistry*; W. B. Saunders Company: Philadelphia, PA, 1977; pp 359−410.
(35) (a) Lever, A. B. P. *Inorganic Electronic Spectroscopy*, 2nd ed.; Elsevier: Amsterdam, 1984; pp 417−429. (b) König, E. *Inorg. Chem.* **1971**, *10*, 2632−2633. (c) Piper, T. S.; Carlin, R. L. *J. Chem. Phys.* **1961**, *35*, 1809−1815.
(36) (a) Figgis, B. N. *Introduction to Ligand Fields*; Interscience Publishers: New York, 1966. (b) Jorgensen, C. K. *Adv. Chem. Phys.* **1963**, *5*, 33−146. (c) Ballhausen, C. J. *Introduction to Ligand Field Theory*; McGraw-Hill Book Co.: New York, 1962.

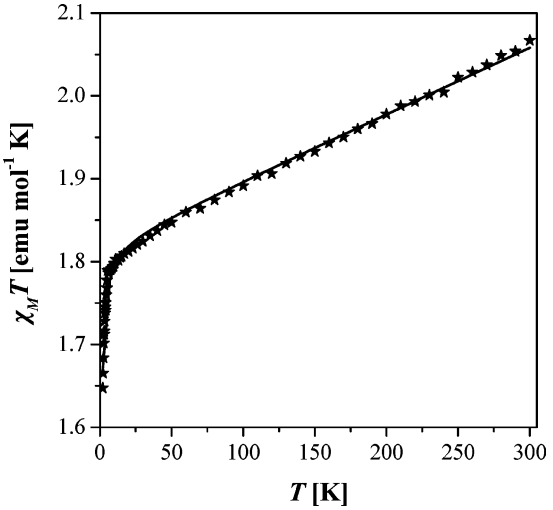

Figure 3. Temperature dependence of the susceptibility data in the form of $\chi_M T$ vs T (solid stars) and the fitting results using the theoretical formula discussed in the text (solid line).

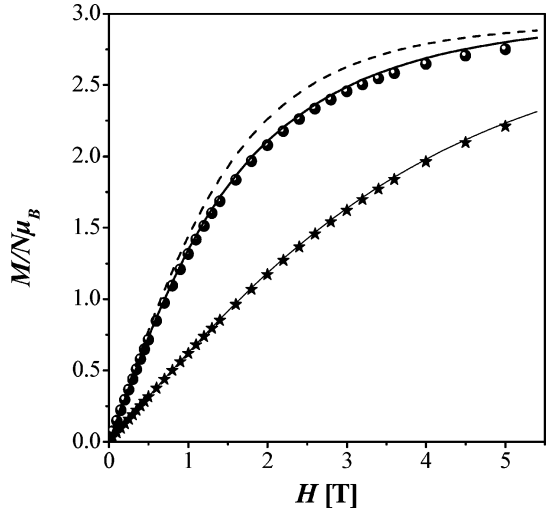

Figure 4. Magnetization measurements in the field range 0−5 T and at temperatures of T = (●) 2 and (★) 5 K. The dotted line represents the theoretical magnetization curve of the $S = {}^3/_2$, $g = 1.97$ system. The solid line represents the addition of a zero-field term $D = 1.0$ cm^{-1}. See text for details.

vibrational status of the citrate ligand upon binding to the chromium ion.[37] The difference between the symmetric and antisymmetric stretches, $\Delta[\nu_{as}(COO^-) - \nu_s(COO^-)]$, was greater than 200 cm^{-1}, indicating that the carboxylate groups of the citrate ligand were either free or coordinated to Cr(III) in a monodentate fashion.[38] This conclusion was subsequently confirmed by the X-ray crystal structure of **1**. All of the above assignments were in agreement with past assignments in mononuclear Cr(III)O_6 complexes[39] and were in line with previous reports on carboxylate containing substrates bound to metal ions of various natures.[40−44]

Magnetic Susceptibility Studies. Magnetic susceptibility measurements were carried out at different magnetic fields and over the temperature range 2−300 K. The temperature dependence of $\chi_M T$ [where χ_M is the magnetic susceptibility for one Cr(III) ion] for complex **1** is shown in Figure 3 (solid stars). The $\chi_M T$ value is 2.05 emu mol^{-1} K at 300 K, higher than the value expected for an isolated ion of Cr(III), i.e., 1.87 emu mol^{-1} K. Up to 10 K there is a smooth linear decrease, whereas after this temperature and up to 2 K, a more pronounced decrease occurs, resulting in a value of 1.65 emu mol^{-1} K. The shape of this curve is characteristic of the occurrence of a very weak antiferromagnetic interaction between abutting Cr(III) centers. That renders important the temperature-independent paramagnetism (TIP) effect and leads to a linear temperature dependence of the susceptibility data. Taking into consideration the one-dimensional character of **1**, the susceptibility data were fitted by the equation

$$\chi_M = \frac{Ng^2\beta^2}{kT}\frac{(A + Bx^2)}{(1 + Cx + Dx^3)} + \text{TIP} \qquad (1)$$

This relationship is based on Weng's[45] numerical results. The coefficients were generated by Hatfield et al.[46] for an $S = {}^3/_2$ antiferromagnetic linear chain, for which $x = |J|/kT$, $A = 1.25$, $B = 17.041$, $C = 6.736$, and $D = 238.47$ and N, g, and β have their usual meanings. The best fit (solid line in Figure 3) is given by the parameters $J = 0.02$ cm^{-1} and $g = 1.96$, yielding TIP $= 800 \times 10^{-6}$, and as indicated above, the emerging coupling is weakly antiferromagnetic.

Isothermal magnetization curves at $T = 2-5$ K in applied fields of 0−5 T are shown in Figure 4. The curves for the increasing and decreasing fields are identical.

The data were simulated using the equation

$$M = Ng\mu_B SB_{3/2}(x) \qquad (2)$$

where $B_{3/2}(x)$ is the theoretical Brillouin function for an $S = {}^3/_2$ system (dotted line). The difference between the experimental and calculated curves at 2 K comes from the single-ion anisotropy of the chromium ion, which is significant at low temperatures. Including the zero-field term in the above model yields a better simulation curve (solid line), with the values $D = 1.0$ cm^{-1} and $g = 1.97$ for both 2 and 5 K.

To confirm this large crystal field parameter, the results of UV−visible spectroscopy were taken into consideration (Figure 2). From the observed band positions of the optical

(37) Deacon, G. B.; Philips, R. *J. Coord. Chem. Rev.* **1980**, *33*, 227−250.
(38) Djordjevic, C.; Lee, M.; Sinn, E. *Inorg. Chem.* **1989**, *28*, 719−723.
(39) Nakamoto, K. *Infrared and Raman Spectra of Inorganic and Coordination Compounds*; 5th ed.; John Wiley and Sons, Inc.: New York, 1997; Part B.
(40) (a) Matzapetakis, M.; Raptopoulou, C. P.; Terzis, A.; Lakatos, A.; Kiss, T.; Salifoglou, A. *Inorg. Chem.* **1999**, *38*, 618−619. (b) Matzapetakis, M.; Raptopoulou, C. P.; Tsohos, A.; Papefthymiou, B.; Moon, N.; Salifoglou, A. *J. Am. Chem. Soc.* **1998**, *120*, 13266−13267. (c) Matzapetakis, M.; Dakanali, M.; Raptopoulou, C. P.; Tangoulis, V.; Terzis, A.; Moon, N.; Giapintzakis, J.; Salifoglou, A. *J. Biol. Inorg. Chem.* **2000**, *5*, 469−474. (d) Matzapetakis, M.; Karligiano, N.; Bino, A.; Dakanali, M.; Raptopoulou, C. P.; Tangoulis, V.; Terzis, A.; Giapintzakis, J.; Salifoglou, A. *Inorg. Chem.* **2000**, *120*, 4044−4051.
(41) Griffith, W. P.; Wickins, T. D. *J. Chem. Soc. A* **1968**, 397−400.
(42) Vuletic, N.; Djordjevic, C. *J. Chem. Soc., Dalton Trans.* **1973**, 1137−1141.
(43) Kaliva, M.; Giannadaki, T.; Raptopoulou, C. P.; Tangoulis, V.; Terzis, A.; Salifoglou, A. *Inorg. Chem.* **2001**, *40*, 3711−3718.
(44) Tsaramyrsi, M.; Kavousanaki, D.; Raptopoulou, C. P.; Terzis, A.; Salifoglou, A. *Inorg. Chim. Acta* **2001**, *320*, 47−59.
(45) Weng, C.-Y. Finite Exchange: Coupled Magnetic Systems. Ph.D. Dissertation, Carnegie-Mellon University, Pittsburgh, PA, 1968.
(46) Hiller, W.; Strähle, J.; Datz, A.; Hanack, M.; Hatfield, W. E.; Ter Haar, L. W.; Gütlich, P. *J. Am. Chem. Soc.* **1984**, *106*, 329.

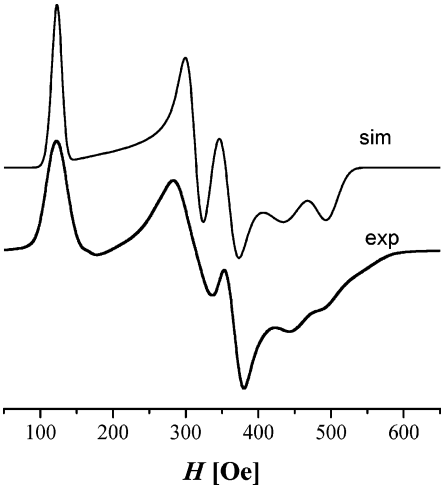

Figure 5. Simulated (sim) and experimental (exp) X-band EPR powder spectra of complex **1** (microwave resonance = 9.43 GHz).

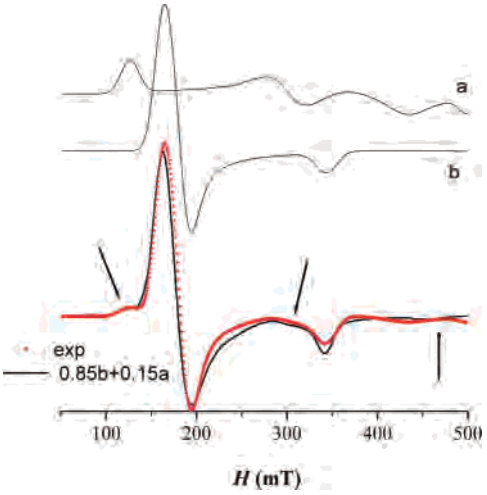

Figure 6. Simulated and experimental X-band EPR frozen solution spectra of complex **1.** Superposition of theoretical spectra a and b gives the spectrum represented by the solid line, and the experimental spectrum (exp) is shown in red triangles forming a thick solid line. See text for details.

absorption spectrum, the values of the crystal field parameter and the Racah interelectronic repulsion parameter B were evaluated. In octahedral symmetry, the energy difference between the $^4A_{2g}$ and $^4T_{2g}$ states is equal to $10Dq$, and hence, Dq can be evaluated using the relation

$$10Dq = E[^4A_{2g}(F) \rightarrow {}^4T_{2g}(F)]$$

The value of the Racah parameter B can be estimated from the position of the two lower-lying absorption bands

$$\frac{Dq}{B} = \frac{15(x-8)}{x^2-10x} \qquad \text{with} \qquad x = \frac{E_1 - E_2}{Dq}$$

where E_1 and E_2 correspond to the energies of the $^4A_{2g}(F) \rightarrow {}^4T_{2g}(F)$ and $^4A_{2g}(F) \rightarrow {}^4T_{1g}(F)$ transitions, respectively.[47]

In weak crystal field sites, values of $Dq/B \ll 2.3$ are found, whereas for strong fields, values of $Dq/B \gg 2.3$ emerge.[48] For intermediate crystal fields, a value of $Dq/B \approx 2.3$ arises. The Dq/B value obtained in the present work was 3.41, which indicates a strong crystal field environment around the metal ion.

EPR Spectroscopy. X-band EPR measurements were carried out in both powder samples and frozen aqueous solutions of **1** and are shown in Figures 5 and 6, respectively. The powder and solution spectra at 4 K were simulated[49] with the following Hamiltonian equation

$$H = D\left[S_z^2 - \frac{1}{3}S(S+1)\right] + E(S_x^2 - S_y^2) + g_z\mu_B H_z S_z + g_x\mu_B H_x S_x + g_y\mu_B H_y S_y$$

for a spin of $S = {}^3/_2$. The simulated spectra are also shown in Figures 5 and 6, respectively.

Solid-State Powder Spectrum. An isotropic magnetic-field domain line width was used for the powder spectrum (lw = 20 G), and the broadness of the spectrum signals reveals the g-strain effects. Gaussian distributions of the principal g values were used, and the results are ($\sigma g_x = \sigma g_y = 0.1$, $\sigma g_z = 0.2$). The principal g values for the powder spectrum are $g_{xy} = 1.96(1)$ and $g_z = 1.98(1)$. The values for the crystal field terms are $D = 1.2(2)$ cm^{-1} and $\lambda = E/D = 0.3$, revealing the rhombic character of the system. Gaussian distributions of the D and E parameters were also used [$\sigma(D) = 0.3$, $\sigma(E) = 0.03$]. The simulation of the powder EPR spectrum of complex **1** verifies the large value of the D parameter, calculated from the simulation of the magnetization curve. Several complexes of Cr(III) have large D values and were calculated through simulations of EPR X-band spectra.[50] To confirm the influence of the D parameter on a rhombic system with $S = {}^3/_2$, various simulated spectra are shown in Figure 7 for different D values.

Solution Spectrum. The effective g values $g \approx 4$ and 2 of the complex are typical of an electronic spin of $S = {}^3/_2$, with moderately large zero-field splitting (ZFS) and small rhombicity parameters ($D > h\nu \approx 0.3$ cm^{-1} at the X-band; $E/D \approx 0$). In this regime of ZFS, the spin quartet is split into two Kramers doublets, $|{}^3/_2, \pm{}^1/_2>$ and $|{}^3/_2, \pm{}^3/_2>$, for virtually all fields applied in the EPR spectrometer, and EPR transitions occur only within these doublets. For $E/D = 0$, only the $m_s = \pm{}^1/_2$ doublet is EPR detectable, whereas the $m_s = \pm{}^3/_2$ doublet is EPR-silent. In this limiting case of large axial ZFS ($D \gg h\nu$, $E/D = 0$), the effective g values for $|{}^3/_2, \pm{}^1/_2>$ would be expected at (a) $g_{\text{perpendicular}} = 2S + 1$ for fields applied in the x and y directions and (b) $g_{\text{parallel}} = 2$ along z, which is in close agreement with the experimental findings. The simulations showed that the experimental line shape cannot be reproduced by a single $S = {}^3/_2$ species with a well-defined value for E/D, even if one employs angle-dependent line shape distributions of the type $W^2 = \sqrt{\sum W_i^2 l_i^2}$, where l_i denotes the direction cosines of the applied field.

(47) Casalboni, M.; Caifardone, V.; Giuli, G.; Izzi, B.; Paris, E.; Prosposito, P. *J. Phys. Condens. Matter* **1996**, *8*, 9059.
(48) Long, X.; Lin, Z.; Hu, Z.; Wang, G.; Han, T. P. J. *J. Alloys Compd.* **2002**, *347*, 52.
(49) Stoll, S. Spectral Simulations in Solid-State EPR. Ph.D. Thesis, ETH Zurich, Switzerand, 2003.
(50) Shaham, N.; Cohen, H.; Meyerstein, D.; Bill, E. *J. Chem. Soc., Dalton Trans.* **2000**, 3082 and references therein.

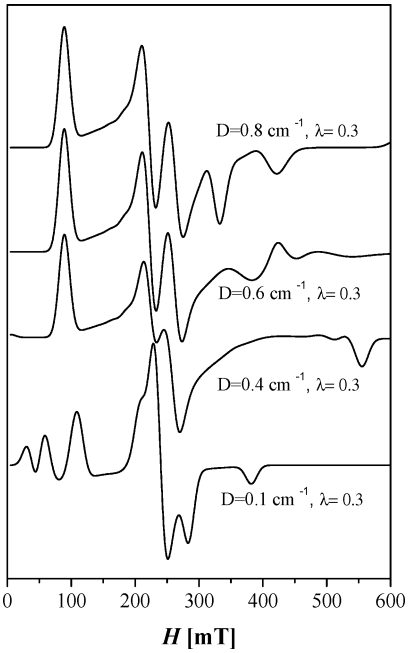

Figure 7. Simulated spectra for a system with $S = {}^3/_2$, $\lambda = 0.3$, and D ranging from 0.1 to 0.8 cm^{-1}. Microwave resonance = 9.6 GHz.

There are well-resolved peaks (shown with arrows in Figure 6) that appear to belong to a different system $S = {}^3/_2$ spins. The well-resolved, narrow small peak at about $g = 5.2$ does not result from an almost forbidden "$\Delta m = 3$" transition within the $m_s = \pm{}^3/_2$ Kramers doublets. Such a feature would be expected to emerge around 5.9. To simulate the actual frozen solution spectrum, a superposition of two different spectra was employed: (a) The first spectrum is a powder "analogue" as described earlier, and (b) the second spectrum is an actual solution simulation. The following conditions were used: An isotropic magnetic-field domain line width was used for the powder spectrum (lw = 25 G), whereas the broadness of the signals in the spectrum revealed the *g*-strain effects. Gaussian distributions of the isotropic *g* value were used ($\sigma g = 0.1$), and the isotropic *g* value for the solution spectrum was $g = 1.96(1)$. The values of the crystal field terms were $D = 1.2(2)$ cm^{-1} and $\lambda = E/D = 0.0$, and the Gaussian distributions of the *D* and *E* parameters were [$\sigma(D) = 0.3$, $\sigma(E) = 0.03$]. The percent contribution of this spectrum to the actual experimental spectrum is 88%, with the remainder belonging to the powder analogue. In Figure 6, the superposition spectrum (from the addition of a and b) is shown (solid line), along with the experimental one. As can be seen, there is a very good match in the simulation of the extra peaks. The experimental data, therefore, seem to suggest that part of the powder sample was not fully dissolved in the water, thus giving rise to extra resonances in the experimental spectrum.

Thermal Studies. The thermal decomposition of the title complex was studied by TGA−DSC under an atmosphere of oxygen. The complex $(NH_4)_4[Cr(C_6H_4O_7)(C_6H_5O_7)]\cdot 3H_2O$ (**1**) is thermally stable up to 90 °C. Above that temperature, an initial process points to the dehydration of **1**, with the release of lattice water between 90 and 160 °C, signifying an endothermic process. The observed weight loss amounts to 11.8%, a value close to the calculated value of 10.0% based on the molecular formula of the title complex. A subsequent process from 160 to 200 °C involves evolution of ammonia. The observed weight loss of 13.0% is close to the calculated value of 12.2%. Then, there are three consecutive steps between 200 and 340 °C involving the decomposition of the organic part of the molecule. No clear plateaus are reached in these stages, suggesting that the derived products are unstable and decompose further. The total weight loss of 85% due to the decomposition of the title complex is reached at 340 °C, with no further loss up to 1000 °C. This value is in good agreement with the calculated weight loss of 86%, derived from the assumption that the product at that temperature (340 °C) is Cr_2O_3. The overall process can be represented as follows

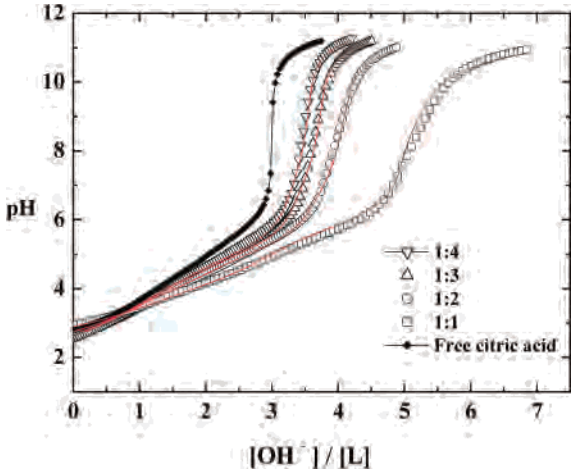

Figure 8. Potentiometric titration curves of (◆) free citric acid (0.003488 M) and chromium(III)−citric acid in molar ratios of (□) 1:1, (○) 1:2, (Δ) 1:3, and (▽) 1:4. Dotted lines reflect experimental curves, and continuous lines reflect calculated curves.

$$2(NH_4)_4[Cr(C_6H_4O_7)(C_6H_5O_7)]\cdot 3H_2O + 18O_2 \rightarrow Cr_2O_3 + 24CO_2 + 8NH_3 + 19H_2O$$

The DSC profile of the complex exhibits clear features that correspond to the aforementioned TGA processes. Collectively, the rather small number of observed processes likely reflects simple mechanisms of decomposition pathways for the title complex.

Speciation Studies. Potentiometric titrations of the citric acid ligand alone and of Cr(III) with citric acid in various metal-ion-to-ligand molar ratios were carried out. Some of the titration curves obtained, both experimental and calculated, are shown in Figure 8. The titration curves were evaluated with different potential speciation models. The best fit between the experimental and calculated titration curves for the binary Cr(III)−citric acid system was obtained by considering the species $[CrLH_3]^{3+}$ ($LH_3 = C_6H_8O_7$), $[CrLH_2]^{2+}$ ($LH_2 = C_6H_7O_7^-$), $[CrLH]^+$ ($LH = C_6H_6O_7^{2-}$), $[CrL]^0$ ($L = C_6H_5O_7^{3-}$), $[CrLH_{-1}]^-$ ($LH_{-1} = C_6H_4O_7^{4-}$), the dinuclear form $[(CrLH_{-1})_2H_{-3}]^{5-}$, $[CrLH_{-2}]^{2-}$, and $[CrL_2H_{-1}]^{4-}$ (water molecules are omitted from the formulas used). The fit is reasonably good in the overall pH and concentration ranges used, demonstrating that the adopted speciation model

Table 3. Proton (log K) and Chromium(III)−Citrate Complex Formation Constants (log β) at $I = 0.15$ M (NaCl) and 25 °C[a]

log K/log β	citric acid	model	pH range for participating species
log K (HL)	5.59(1)		
log K (H_2L)	4.32(1)		
log K (H_3L)	2.94(1)		
log β ($CrLH_3$)		19.01(4)	<4
log β ($CrLH_2$)		16.34(4)	2.5−5
log β (CrLH)		12.54(4)	2.5−5.5
log β (CrL)		8.18(4)	3−6.5
log β ($CrLH_{-1}$)		2.56(4)	4−8.5
log β ($CrLH_{-2}$)		−3.51(3)	5−11
log β (CrL_2H_{-1})		6.13(4)	4−8.5
log β ($Cr_2L_2H_{-5}$)		−13.30(6)	>7
number of points		501	
fitting parameter[b]		0.0288	
log β_{113} − log β_{3a}		6.16	
log β_{112} − log β_{2a}		6.43	
log β_{111} − log β_{1a}		6.95	

[a] Charges from the various species are omitted for reasons of clarity. [b] Goodness of fit between the experimental and the calculated titration curves, expressed in mL of titrant.

is satisfactorily defined. Other complexes, such as 1:3 Cr(III)-citrate complexes or variably protonated and deprotonated species, were rejected by the computer program (PSEQUAD) during the calculation process (computation). The species emerging from the speciation distribution of the binary system are in good agreement with the corresponding species synthesized and isolated in the solid state. The stability constants of the complexes formed are listed in Table 3. The uncertainties (3SD values) of the stability constants are given in parentheses. The pH ranges of their optimal formation are also reported. For the three titratable citrate carboxylate groups, the pK_a values of 5.59, 4.32, and 2.94 were obtained and found to be very close to the values reported by Kotsakis et al.[51] at 0.2 M ionic strength (5.59, 4.26, and 2.87, respectively).

The titrimetric data were evaluated on the premise that complex formation between Cr(III) and citrate proceeds through binding of the citrate carboxylate moieties and the alkoxide group. The titration curves in the absence and presence of Cr(III) suggest clearly the formation of the mononuclear complexes $[CrLH_3]^{3+}$, $[CrLH_2]^{2+}$, $[CrLH]^{+}$, and $[CrL]^{0}$ in the acidic region up to pH 4.5. The latter species contains a triply deprotonated citrate ligand bound to the metal ion. As the pH of the aqueous solution increases, more mononuclear species such as $[CrLH_{-1}]^{-}$, $[CrL_2H_{-1}]^{4-}$, and $[CrLH_{-2}]^{2-}$ emerge with the predominant species in the lower part of the pH range of 4.5−7 being $[CrLH_{-1}]^{-}$, $[CrL_2H_{-1}]^{4-}$ = $[Cr(C_6H_5O_7)(C_6H_4O_7)]^{4-}$, and gradually switching to $[CrLH_{-2}]^{2-}$. The $[CrLH_{-1}]^{-}$ species contains a quadruply deprotonated citrate ligand bound to the metal ion, whereas the $[CrL_2H_{-1}]^{4-}$ species contains one triply and one fully deprotonated citrate bound to Cr(III). A 1:2 Cr(III)-to-citrate stoichiometry suggests an octahedral geometry for the $[Cr(C_6H_5O_7)(C_6H_4O_7)]^{4-}$ species. The binding mode of the citrate ligands could be either through the three carboxylate groups or through one of the terminal carboxylates, the central carboxylate, and the alkoxide group, whereas the remaining terminal carboxylate group does not enter the coordination sphere of Cr(III). It appears that the tridentate coordination of citrate through the three carboxylate groups is not preferred for other divalent or trivalent metal ions, such as Cu(II),[52] Co(II),[51] Al(III),[53] and VO(II).[54] In contrast to the tridentate carboxylate coordination mode, mentioned above, appears to be the coordination mode encountered in the synthesized and isolated species $[Cr(C_6H_5O_7)(C_6H_4O_7)]^{4-}$. The same mode of citrate coordination applies to the $[CrLH_{-2}]^{2-}$ species. The additional proton in $[CrLH_{-2}]^{2-}$ emerges upon dissociation of a coordinated water molecule from $[CrLH_{-1}]^{-}$. Considering the data in this pH range, it appears that $\log[K(CrL_2H_{-1})/K(CrLH_{-1})] \approx 1$. This value indicates a favorable formation constant for $[Cr(C_6H_5O_7)(C_6H_4O_7)]^{4-}$ compared to $[Cr(C_6H_4O_7)]^{-}$. In fact, the two species coexist in the same pH range, with the former comprising 50% of the total Cr(III) fraction compared to ∼20% for the latter species at pH ≈ 6 (Figure 9).

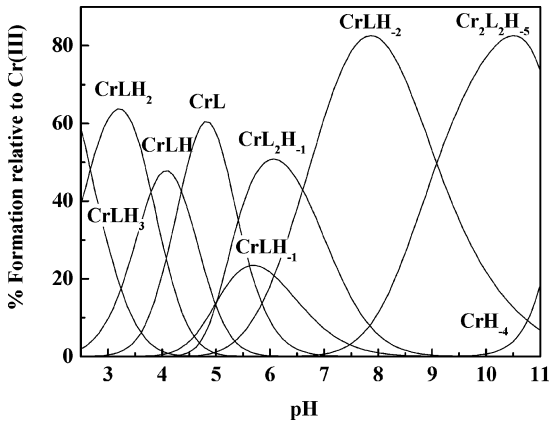

Figure 9. Speciation curves for complexes forming in the Cr(III)−citric acid system (c_{Cr} = 0.001698 mol dm^{-3}, c_{ligand} = 0.003488 mol dm^{-3}). Charges are omitted for clarity.

In the high-pH region, beyond 7, species such as $[(CrLH_{-1})_2H_{-3}]^{5-}$, $[CrLH_{-2}]^{2-}$, and $[CrH_{-4}]^{-}$ appear, both mononuclear and dinuclear in nature. In the lower end of this pH range, the mononuclear species, having emerged from the higher end of the pH 4.5−7 range, is the predominant species, reaching over 80% of the Cr(III) species distribution at pH 8. At higher pH values, the predominant species is the dinuclear species $[(CrLH_{-1})_2H_{-3}]^{5-}$, with $[CrH_{-4}]^{-}$ = $[Cr(OH)_4]^{-}$ ($\log \beta_{1-4} = -27.8$) being the minor species toward the high end of the investigated pH range. It is worth noting that the dinuclear species might originate from the previously emerging $[CrLH_{-1}]^{-}$ species, for which a clear picture of the coordination mode of citrate was proposed. On these grounds, dinuclear complex formation through the mononuclear species could be forged via further consideration of (a) employment of the noncoordinated citrate

(51) Kotsakis, N.; Raptopoulou, C. P.; Tangoulis, V.; Terzis, A.; Giapintzakis, J.; Jakusch, T.; Kiss, T.; Salifoglou, A. *Inorg. Chem.* **2003**, *42*, 22−31.

(52) Kiss, E.; Kiss, T.; Jezowska-Bojczuk, M. *J. Coord. Chem.* **1996**, *40*, 157−166.

(53) Lakatos, A.; Bányai, I.; Bertani, R.; Decock, P.; Kiss, T. *Eur. J. Inorg. Chem.* **2001**, 461−469.

(54) Kiss, T.; Buglyo, P.; Sanna, D.; Micera, G.; Decock, P.; Dewaele, D. *Inorg. Chim. Acta* **1995**, *239*, 145−153.

terminal carboxylate group in binding to an adjacent $[CrLH_{-1}]^-$ species unit (and vice versa) and/or (b) deprotonation of coordinated water molecule(s), leading to OH^- moieties potentially acting as bridges to the adjacently located $[CrLH_{-1}]^-$ units. Taking into account the fact that the first hydrolysis constant of $[Cr(OH_2)_6]^{3+}$ is p$K = 4.0$ and that of the $[CrLH_{-1}]^-$ species is p$K \approx 6.0$, it is apparent that there is a significant decrease in the acidity of the coordinated water molecule(s) in the $[CrLH_{-1}]^-$ species. Therefore, as the pH of the reaction solution increases, a metal-bound water molecule in $[CrLH_{-1}]^-$ could likely be deprotonated, with the emerging OH^- moiety(ies) acting as a bridge to an adjacent $[CrLH_{-1}]^-$ unit, promoting hydroxo-bridged dinuclear assembly formation. This conclusion is in line with the fact that hydroxo and dihydroxo bridges are a characteristic feature in Cr(III) complexation chemistry, leading to dinuclear species. Representative examples of such species are the complexes $[(H_2O)_4Cr(OH)_2Cr(H_2O)_4]^{4+}$,[55] $[Cr(phen)_2(OH)]_2Cl_4\cdot 6H_2O$,[56] $[Cr(tpa)(OH)]_2(ClO_4)_4\cdot 4H_2O$,[57] $[Cr(gly)_2(OH)]_2$,[58] and $[Cr(pic)_2(OH)]_2^{4+}$[59] already reported in the literature. Analogous chemistry has been observed in the cases of Cu(II), Al(III), and VO(II).

Discussion

A Closer Look at the Chemistry and the Species in Cr(III) Aqueous Speciation. The current investigation of the binary Cr(III)−citrate system led to the expedient synthesis of the mononuclear chromium−citrate species $(NH_4)_4[Cr(C_6H_4O_7)(C_6H_5O_7)]\cdot 3H_2O$ (**1**). Two major points are worth noting in this work: (a) The species synthesized and isolated at a specific pH (5.5) emerged as a Cr(III) complex with two citrate ligands attached to it in the same fashion, yet with different states of (de)protonation. (b) The site of (de)protonation was one of the terminal carboxylate groups of the metal-bound citrate ligand.

The structural characterization of **1** showed that Cr(III), a rather kinetically inert metal ion, behaves similarly to other trivalent metal ions in its aqueous chemistry with α-hydroxycarboxylic acids, such as citric acid. In fact, the nature of the isolated complex **1** is the same as that of the Al(III) and Ga(III) systems already studied synthetically and structurally. In this sense, the mixed protonation state of bound citrate ligands around the trivalent metal ions becomes a common feature of the structural speciation of the requisite binary M(III)−citrate [M(III) = Cr(III), Al(III), Ga(III)] system. Characteristic examples of relevant anionic complexes include $[Al(C_6H_4O_7)_2]^{5-}$,[40a] $[Al(C_6H_4O_7)(C_6H_5O_7)]^{4-}$,[26] $[Ga(C_6H_4O_7)(C_6H_5O_7)]^{4-}$,[26] $[Fe(C_6H_4O_7)_2]^{5-}$,[40b] $[Mn(C_6H_4O_7)_2]^{5-}$,[40d] and $[Mn(C_6H_5O_7)_2]^{4-}$.[40d] Hence, it is very likely that analogous species containing fully deprotonated citrate ligands bound to the Cr(III) ion exist. The synthesis and isolation of such species is currently being pursued in our laboratories.

The derived alkoxide group participates in the formation of the five-membered metallacyclic ring, which further stabilizes the entire mononuclear complex. A similar behavior was observed for other trivalent metal ions such as Al(III), Ga(III), Mn(III), and Fe(III) in aqueous binary systems with citric acid. This is in contrast to the congener complexes of citrate with divalent metal ions, in which the alcoholic moiety in the five-membered metallacyclic ring remains protonated. Contrasting the structural observations for **1** seems to be the case of the only other reported complex $(C_5H_6N)_2[Cr(C_6H_{5.5}O_7)_2]\cdot 4H_2O$,[27] in which the alkoxide groups of the two citrate ligands appear to share a proton (half-occupancy), thus projecting partial deprotonation of the requisite moiety in the presence of the trivalent metal ion Cr(III). Ostensibly, more Cr(III)−citrate pH-structural variants need to be characterized crystallographically, in analogy with complexes of other trivalent metal ions, to unequivocally assign the (de)protonation state of the alcoholic moiety bound to Cr(III). Such pH-specific synthetic efforts are currently ongoing.

The aforementioned structural attributes of the citrate ligand environment of Cr(III) in **1** reflect quite well the arising spectroscopic properties of the species in the solid state and in solution. In this context, the electronic spectroscopy characteristics of the complex conform to the results of EPR spectroscopy and project the properties of **1** in the solid state and in solution as a mononuclear species with a distinct structure. Moreover, the magnetic susceptibility studies on **1** reveal characteristics of its magnetic behavior, which is consistent with its EPR spectroscopic and structural signatures.

The synthetic structural speciation attempted here at the specific pH of 5.5 is but a first step toward completing the investigation of pH-variant chromium(III)−citrate species present in aqueous media. Knowledge of (a) the nature of the species present and (b) the physical and chemical properties of the speciation participants will undoubtedly contribute to the understanding of the bioavailability of Cr(III) as a prerequisite for (i) its biochemical interactions with low- and high-molecular-mass biomolecular targets and (ii) any subsequent biological influences and/or beneficial and detrimental toxicity effects that it might have on cellular integrity.

Speciation Studies on the Binary System. The aqueous speciation in the binary Cr(III)−citric acid system is reflected in the speciation curves depicted in Figure 9. The speciation can be described satisfactorily by considering the presence of both (a) 1:1 chromium−citrate complexes in the protonated form $[CrLH_n]^{n+}$ ($n = 1-3$), deprotonated form $[CrL]^0$, and fully deprotonated form $[CrLH_{-m}]^{m-}$ ($m = 1, 2$) and (b) 1:2 deprotonated mononuclear Cr(III)−citrate species $[CrL_2H_{-1}]^{4-}$. Also, at high pH values, the fully deprotonated dinuclear form $[(CrLH_{-1})_2H_{-3}]^{5-}$ emerges. As can be seen from the speciation curves, the solid-state compound syn-

(55) (a) Spiccia, L.; Stoeckli-Evans, H.; Marty, W.; Giovanoli, R. *Inorg. Chem.* **1987**, *26*, 474−482. (b) Laswick, J. A.; Plane, R. A. *J. Am. Chem. Soc.* **1959**, *81*, 3564.
(56) Veal, J. T.; Hatfield, W. E.; Hodgson, D. J. *Acta Crystallogr. E* **1973**, *29*, 12.
(57) Hodgson, D. J.; Zietlow, M. H.; Pedersen, E.; Toftlund, H. *Inorg. Chim. Acta* **1988**, *149*, 111−117.
(58) (a) Veal, J. T.; Hatfield, W. E.; Jeter, D. Y.; Hempel, J. C.; Hodgson, D. J. *Inorg. Chem.* **1973**, *12*, 342. (b) Veal, J. T.; Jeter, D. Y.; Hempel, J. C.; Eckberg, R. P.; Hatfield, W. E.; Modgson, D. J. *Inorg. Chem.* **1973**, *12*, 2928 (footnote 44).
(59) Michelsen, K. *Acta Chem. Stand., Ser. A* **1976**, *30*, 521.

Table 4. Logarithms of Citrate Equilibrium Constants for Al(III), Fe(III), and Cr(III)

reaction	log K Al(III)[62]	log K Fe(III)[62]	log K Cr(III)
$M^{3+} + LH^{2-} \rightleftarrows MLH^{+}$	4.7	6.7	6.95
$MLH^{+} \rightleftarrows ML^{o} + H^{+}$	−2.5	−1.3	−4.36
$M^{3+} + L^{3-} \rightleftarrows ML^{o}$	8.0	11.2	8.18
$ML^{o} \rightleftarrows MLH_{-1}^{-1} + H^{+}$	−3.4	−2.8	−5.62

thesized and isolated at pH 5.5 appears to be 50% of the total species fraction in solution around pH ≈ 6. The deprotonated species $[CrLH_{-2}]^{2-}$ represents 80% of the total species fraction in solution around pH ≈ 8. At basic pH, a deprotonated dinuclear chromium(III)−citrate complex appears. A similar dinuclear iron(III)−citrate species in the deprotonated form was proposed by Spiro et al. [60] at high pH for the binary Fe(III)−citric acid system.

An examination of the stepwise deprotonation constants pK($CrLH_n$) ($n = -1, 0, 1, 2, 3$) in Table 4 suggests that all $CrLH_n$ complexes are chelated.[61] In fact, partial formation constants (log K values expressed as log β_{11n} − log β_{na} in Table 4) calculated for the process $Cr^{3+} + H_nL^{n-3} \rightleftarrows [CrLH_n]^n$ are greater than 6.0, indicating chelated ligands.[61] A similar conclusion was reached in the case of V(IV) complexes and phosphonated derivatives of NTA.[61]

A comparison of chromium(III)−citrate equilibrium constant logarithms with corresponding constants for aluminum and iron(III) (Table 4) suggests similar stabilities for some of the 1:1 M(III)−citrate (M = Cr, Al, Fe) complexes.[62]

Cr(III) Solubility and Potential Toxicity. Chromium is present in a variety of environments, including forest soils and sediments,[63] leather tanning plants and laboratories, and surface and atmospheric waters. Albeit nutritionally essential as a micronutrient, chromium has the potential to influence biological processes, exerting cytotoxic as well as genotoxic and carcinogenic activities.[64−67] Two thermodynamically stable states mainly exist in the various environments where chromium is found, namely, Cr(III) and Cr(VI). Of these, Cr(VI) poses a significant health hazard to the living world. Cr(III), on the other hand, is a low-oxidation-state ionic form toward which the reduction of Cr(VI) entering biological fluids generates reactive species, including radicals,[68,69] that damage DNA and other cellular components. In all such cases, soluble Cr(III) is key to understanding its aqueous chemistry with intracellular substrates, such as α-hydroxycarboxylates and protein components, and any subsequent toxic repercussions that it potentially brings within the cellular environment. Given that solubility begets bioavailability and bioavailability is strongly associated with toxic effects, the presence of well-characterized forms of Cr(III) contribute to (a) further understanding of the early steps of toxicologically significant chemical events and (b) linking of initial key metal ionic forms of chromium with ultimate damage at the cellular level.

In the present case, the pursued pH-specific chemistry of the binary system Cr(III)−citric acid afforded soluble species that could be isolated in pure crystalline form, studied comprehensively, and characterized fully. As a result, the spectroscopic and structural characterization of **1** in the solid state and in solution projected a fingerprint signature of a soluble binary chromium(III)−citrate species. Therefore, key physicochemical properties of chromium(III)−hydroxycarboxylate species emerge as fundamental attributes that could be factored into (a) the design and development of methodologies for the sensitive and selective determination[70] of that metal ion in a variety of aqueous media (environment, bacteria, plants, humans), thus signifying efforts to diagnose and prevent detrimental biological effects of chromium in living organisms, and (b) the examination of Cr(III) toxicity in biologically relevant fluids and the assessment of its potential to induce damage to cellular components and structures. The aforementioned goals seem tangible when both the presence of Cr(III) under physiologically (and/or aberrant) relevant conditions and well-defined Cr(III) competitive—albeit diversely complex—interactions with key cellular targets (e.g., proteins, DNA) are taken into consideration.

Chromium(III) Carboxylate Species as Precursors to New Materials. Chromium has been known to be a component of various types of materials including (a) binary Cr/W oxide thin films for potential applications in gas sensing,[71] (b) Cr-substituted hematites and magnetite materials relevant to the removal of corrosion products-deposits on iron-based alloys in pressurized water reactors,[72] and (c) mixed oxides of the type $La_{0.9}Sr_{0.1}Ni_{1-x}Cr_xO_3$ with a perovskite structure.[73] Materials, such as perovskite phases, are prepared by the citrate method and used as catalysts involving H_2O_2 decomposition. This method makes use of complexes not unlike the one prepared here. Therefore, well-defined species such as **1** could serve as precursors for the synthesis of new materials.

(60) Spiro, T. G.; Pape, L.; Saltman, P. *J. Am. Chem. Soc.* **1989**, *89*, 5555−5559.
(61) Sanna, D.; Bodi, I; Bouhsina, S.; Micera, G.; Kiss, T. *J. Chem. Soc., Dalton Trans.* **1999**, 3275−3282.
(62) Martin, R. B. *J. Inorg. Biochem.* **1986**, *28*, 181−187.
(63) Flogeac, K.; Guillon, E.; Aplincourt, M. *J. Colloid Interface Sci.* **2005**, 286, 596.
(64) Zhitkovich, A.; Song, Y.; Quievryn, G.; Voitkun, V. *Biochemistry* **2001**, *40*, 549−560.
(65) (a) Wu, F.-Y.; Wu, W.-Y.; Kuo, H.-W.; Liu, C.-S.; Wang, R.-Y.; Lai, J.-S. *Sci. Total Environ.* **2001**, *279*, 21−28. (b) Kortenkamp, A.; Casadevall, M.; Da Cruz Fresco, P.; Shayer, R. O. J. *NATO ASI Ser. 2* **1997**, *26*, 15−34. (c) Borges, K. M.; Wetterhahn, K. E. *Carcinogenesis* **1989**, *10*, 2165−2168.
(66) Goodgame, D. M. L.; Joy, A. M. *J. Inorg. Biochem.* **1986**, *26*, 219−224.
(67) Koutras, G. A.; Hattori, J.; Schneider, A. S., Jr.; Ebaugh, F. G.; Valentine, W. N. *J. Clin. Invest.* **1964**, *43*, 323−331.
(68) (a) Speetjens, J. K.; Collins, R. A.; Vincent, J. B.; Woski, S. A. *Chem. Res. Toxicol.* **1999**, *12*, 483−487. (b) Sugden, K. D.; Geer, R. D.; Rogers, S. J. *Biochemistry* **1992**, *31*, 11626−11631.
(69) Aiyar, J.; Berkovits, H. J.; Floyd, R. A.; Wetterhahn, K. E. *Environ. Health Perspect.* **1991**, *92*, 53−62.
(70) Massumi, A.; Najafi, N. M.; Barzegari, H. *Microchem. J.* **2002**, *72*, 93−101.
(71) Cantalini, C. *J. Eur. Ceram. Soc.* **2004**, *24*, 1421−1424.
(72) (a) Manjanna, J.; Venkateswaran, G. *Hydrometallurgy* **2001**, *61*, 45−63. (b) Manjanna, J.; Venkateswaran, G.; Sherigara, B. S.; Nayak, P. V. *Hydrometallurgy* **2001**, *60*, 155−165.
(73) Ariafard, A.; Aghabozorg, H. R.; Salehirad, F. *Catal. Commun.* **2003**, *4*, 561−566.

Conclusions

The diversity of chromium applications and health effects requires that soluble and bioavailable species be known and their structural and physicochemical properties be determined. Linked to these aspects are the connections of the relevant aqueous chemistry of the metal, in its prevalent ionic forms, with the influence it exerts on biological and nonbiological processes as a chemical reagent/participant. To this end, the delineation of the aqueous distribution of Cr(III)-L (L = organic substrate) species as a function of the concentrations of the reagents involved and their molecular formula is a significant challenge. In the case of Cr(III), which is one of the two predominant ionic forms of chromium in nature, the pH-specific synthesis of complex **1** reflects a focused effort to delineate the structural speciation of the binary Cr(III)−citrate system, with the citrate ligand being a low-molecular-mass physiological agent of many structural and chemical attribute, promoting its chemical reactivity toward metal ions. Without discounting the importance of binary and ternary interactions of Cr(III) with high-molecular-mass cellular targets, the nature and physicochemical properties of **1** in the solid state and in solution are but the first step in understanding the complex distribution of binary chromium(III)−citrate species and the related interactions under variable conditions dictated by a plethora of factors and biological settings. Hence, the contribution of the pH-dependent synthetic chemistry in the exploration of (a) Cr(III)-L relevant chemistries and (b) areas extending from the environmental pollution to advanced materials preparation and to biotoxic effects in humans is significant, in view of the fact that solution studies on specific Cr(III)-L binary systems do not currently exist. Given that well-characterized forms of Cr(III) in the presence of citrate are likely involved in chemical processes, underlying physiological and toxic manifestations related to the metal ion's activity in biological media, further synthetic studies targeting such species along with pertinent solution studies on the requisite binary systems will undoubtedly shed light on the issue. Studies along these lines are currently in progress in our laboratories.

Acknowledgment. This work was supported by a "Pythagoras" grant from the National Ministry of Education and Religious Affairs and by a "PENED" grant from the General Secretariat of Research and Technology, Greece.

Supporting Information Available: X-ray crystallographic files, listings of positional and thermal parameters, and H-bond distances and angles for **1**. The material is available free of charge via the Internet at http://pubs.acs.org.

IC061480J